Hydrodynamics and particle motion in upward flowing dense particle suspensions: Application in solar receivers

P. García-Triñanes, J.P.K. Seville, B. Boissière, R. Ansart, T.W. Leadbeater, D.J. Parker

Chemical Engineering Science

www.elsevier.com/locate/ces

PII: S0009-2509(16)30110-5
DOI: http://dx.doi.org/10.1016/j.ces.2016.03.006
Reference: CES12842

To appear in: *Chemical Engineering Science*

Received date: 24 September 2015
Revised date: 9 February 2016
Accepted date: 4 March 2016

Cite this article as: P. García-Triñanes, J.P.K. Seville, B. Boissière, R. Ansart, T.W. Leadbeater and D.J. Parker, Hydrodynamics and particle motion in upwarc flowing dense particle suspensions: Application in solar receivers, *Chemica Engineering Science,* http://dx.doi.org/10.1016/j.ces.2016.03.006

Hydrodynamics and particle motion in upward flowing dense particle suspensions: Application in solar receivers

P. García-Triñanes[1,*], J.P.K. Seville[1], B. Boissière[2,3], R. Ansart[2,3],

T.W. Leadbeater[4], D.J. Parker[4]

[1] *Department of Chemical and Process Engineering [J2], University of Surrey, Guildford, GU2 7XH, United Kingdom*

[2] *Université de Toulouse; INPT, UPS; Laboratoire de Génie Chimique; 4, Allée Emile Monso, F-31030 Toulouse, France*

[3] *CNRS; Laboratoire de Génie Chimique; F-31030 Toulouse, France*

[4] *Positron Imaging Centre, School of Physics and Astronomy, University of Birmingham, Edgbaston, Birmingham, B15 2TT, United Kingdom*

Abstract

Dense gas-solid suspensions have the potential to be applied as heat transfer fluids (HTF) for energy collection and storage in concentrated solar power plants. At the heart of these systems is the solar receiver, composed of a bundle of tubes which contain the solid suspension used as the thermal energy carrier. In the design investigated here, the particles form a dense upward-flowing suspension. The density of the suspension of these particles and their movement each has a strong influence on the heat transfer. An apparatus was designed to replicate at ambient temperature the hydrodynamic and particle motion in the real solar energy plant. The governing parameters of the flow were established as the solid feeding flow rate, the fluidisation velocity, the solids holdup, the freeboard pressure and the secondary air injection (aeration) velocity. In the case studied, aeration was applied, with air introduced into the uplift transport tube some way up its length. This study finds that the amount of this secondary air injection is the most important parameter for the stability and the uniform distribution of the solids flow in the tubes. Solids motion was measured using the non-invasive positron emission particle tracking (PEPT) technique to follow the movement of a 60 µm tracer particle, onto which was adsorbed the positron emitting ^{18}F radioisotope. Analysis of the resulting three-dimensional trajectories provides information on solids flow pattern and solids velocity. Results show the overall behaviour of the bulk material in detail: small step-wise movements associated with bubble motion superimposed on a general trend of upward flow in the centre and downward flow close to the walls. These findings suggest that this particular type of flow is ideal for transporting energy from the walls of the solar receiver tubes.

*Corresponding author: p.garcia@surrey.ac.uk

Graphical Abstract

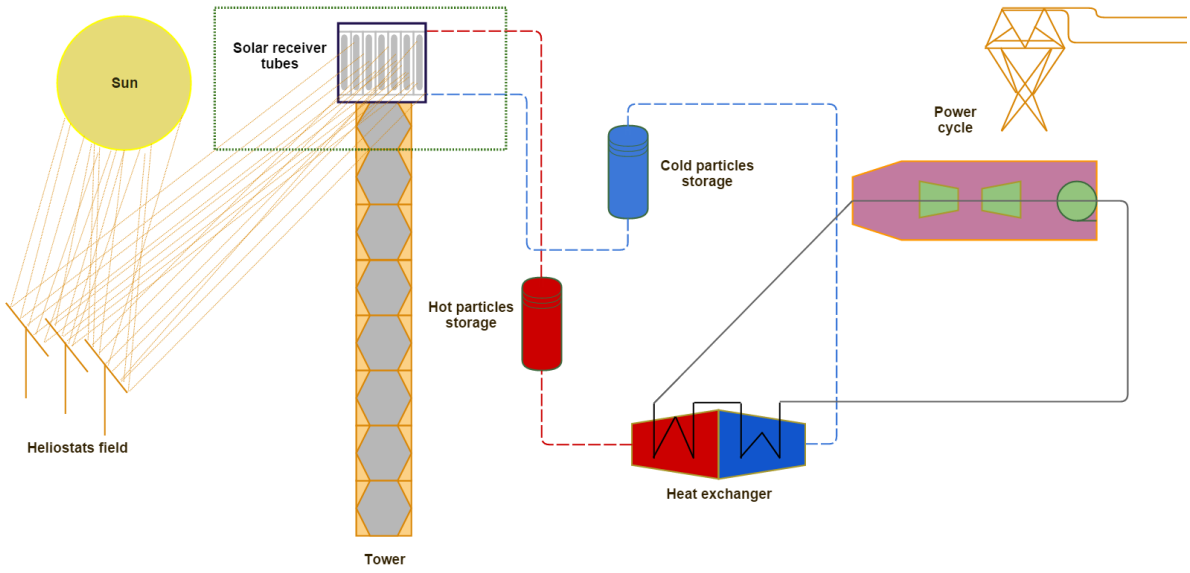

Keywords:

Fluidisation, fine particles (A/B-type), dense particle suspension, upward flow, heat transfer media, solar energy, Positron Emission Particle Tracking

1. Introduction

Concentrated solar energy has received much attention in recent years due to its potential economic return, energy supply impact, and environmental benefits. In concentrated solar power plants, solar energy is focussed by means of arrays of sun-tracking mirrors onto a tower receiver, which is usually a set of tubes through which a heat transfer medium flows WO/2012/052661. The medium is heated and can then exchange this heat with a conventional steam cycle to generate power. The choice of the heat transfer medium is important since it is one of the critical components for storing and transferring thermal energy in **concentrated solar power systems**. Molten salts are traditionally used, but have major disadvantages. These include, for example, the large electricity demand associated with pumping the salt to the top of the tower, practical upper temperature limit, maintenance costs, corrosion, spillage, toxicity and safety issues.

An alternative approach is necessary and we propose the use of a suspension of particulate solids as an advantageous heat transfer medium. In solar energy capture systems, the heat is captured at the outside tube wall, and subsequently transferred to the circulating solids. Few studies have been reported on dense-phase transport of this kind, in which particle motion is constrained by the high degree of particle-particle contact. This is recognised as a difficult regime in which to maintain stable flow conditions due to difficulties ranging from “choking out” (particles dropping out of suspension) to severe slugging, even when sufficient blower pressure and solids feeding are provided (Bi and Grace, 1995).

This particular type of flow is distinct from that normally encountered in conventional circulating fluidised beds. In these beds the gas velocity is much higher and the solids are normally in a dilute suspension, either uniformly across the tube or in a combination of a dense annulus near the wall and a dilute core, with exchange between them.

In general, gas-solid suspensions can be classified according to their particle concentration distribution and to the differences in gas and particle phase movement; bubbling fluidisation, fast fluidisation and dilute phase pneumatic conveying are recognised as distinct states. Since the particles are moving relative to each other and there is great agitation, heat transfer from solid to gas in the dense phase should be higher than in a fixed bed at the same gas velocity and void fraction. However, the particle Reynolds numbers are often less than 1, and fixed bed correlations are not reliable in this region.

The concentration of particles and their motion play a decisive role in the heat transfer and are directly affected by the operating parameters (i.e. gas velocity, bed pressure, bed temperature). Particle convection to the wall is the dominant heat transfer mechanism (Flamant et al., 1992), and the extent of this depends on the local solids density and the rate at which particles are replaced at the wall (i.e. their renewal rate). An increase in gas velocity affects these two parameters in different ways; as the gas velocity is increased, the heat transfer coefficient rises because of the increased renewal of solids at the surface, reaches a maximum and subsequently decreases as the surfaces become blanketed by excess gas (Botterill, 1975).

The conditions for stable flow of particles in these suspensions have been established by previous work at the University of Toulouse (Boissiere et al., 2015). For the present investigations, experiments were carried out at the Positron Imaging Centre (University of Birmingham, Birmingham, UK), using an ambient temperature model constructed specially for this purpose and

reproducing the conditions of the Toulouse experiments. In order to obtain sufficient experimental data it was necessary to operate this apparatus in a **continuous circulation** mode so that sufficient passes of the radioactive tracer could be observed. For this reason a return leg was designed so that solids could circulate in a closed-loop. A stable solids flow was obtained by the same method as employed in the previous work, i.e. by submerging the bottom end of the conveying tube into a slightly pressurised fluidised bed. The solids fraction in the tube is close to that of a dense fluidised bed and a bubbling regime is ensured by its aeration (Flamant et al. 2014).

The present work improves on the understanding of the hydrodynamics in dense upward-flowing gas-particle suspensions by **quantitative characterization** of single particle motion in the solids flow. We describe the particle motion in a vertical tube of the same diameter as those used in a solar receiver, investigated through the use of the Positron Emission Particle Tracking (PEPT) measurement technique and providing a comprehensive description of how the particles behave inside the uplift transport tubes. Since the movement of the particles controls the effective thermal conductivity of the suspension, the particle velocities were determined under a range of conditions in order to quantify the exchange rate between the wall and the bulk of the suspension.

2. Experimental

The selection of the particulate solid was based on its size and its other physical properties. In this application, the powder must have good heat capacity, capability of working at a high temperature (over 750 ˚C), good thermal conductivity, very low attrition and low cost. In addition the absence of any phase transition or chemical reaction in the temperature range of interest is favoured. Based on these criteria, silicon carbide was selected (*Navarro SiC S.A.).* A 100x magnification SEM image of the selected solid (designated F220) is shown in Figure 1.

The particle size must favour good fluidisation at low gas velocities, meaning low gas-compression energy consumption in the solar application. The association of requirements suggests a choice of size and density corresponding to particles that straddle the boundary between A and B groups of Geldart's classification. In practice, a size of 60 µm was found suitable considering that the particle density of F220 silicon carbide is 3210 $kg.m^{-3}$. Volume-based and cumulative particle size distribution measured using a Mastersizer 2000 (*Malvern Instruments Ltd*) are shown in Figure 2.

The minimum fluidisation velocity U_{mf}, the minimum bubbling velocity U_{mb} and their associated void fractions ε_{mf} and ε_{mb} were experimentally determined in a separate column using standard techniques (Seville et al, 1987) and are reported in Table 1.

Table 1: Physical and hydrodynamic properties of F220 silicon carbide.

Physical properties									**Hydrodynamic properties**			
d_{10} [µm]	d_{50} [µm]	d_{90} [µm]	d_{32} [µm]	ρ_p [$kg.m^{-3}$]	λ [$W.m^{-1}.K^{-1}$]	$c_{p,m}$ [$kJ.kg^{-1}.K^{-1}$]	$T_{melting}$ [K]	T_{max} [K]	U_{mf} [$m.s^{-1}$]	ε_{mf}	U_{mb} [$m.s^{-1}$]	ε_{mb}
44	79	130	64	3210	114 (300K) 35 (1300K)	0.67 (300K) 1.26 (1300K)	2730	1300	0.005	0.57	0.008	0.59

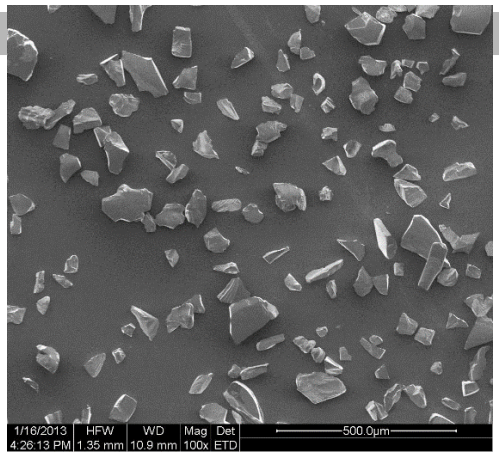

Fig 1. Scanning electron microscopy picture corresponding to the SiC powder sample.

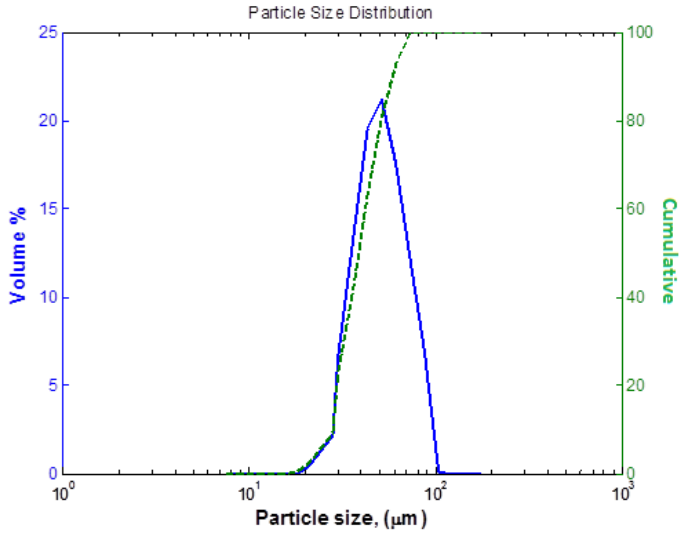

Fig 2. Particle size distribution of the SiC powder.

In the application, the heat transfer medium flows through multiple parallel vertical tubes. In the present study, a single tube with similar dimensions, aeration conditions and a configuration that mimics the receiver concept was used to circulate the powder at ambient temperature for detailed examination of particle motion (shown in Figure 3). The vertical tube of 1.1 m in length and 0.03 m in diameter was partially submerged in a bubbling fluidised bed known as the dispenser fluidised bed (DiFB). For upward flow to occur in the tube, the DiFB must be pressurised, this pressurisation being controlled by use of a *Bronkhorst* type pneumatic valve that uses an integrated pressure control connected to a PID controller.

The dense upward-flowing suspension rises up the transport tube, which has additional aeration located 0.25 m above the bottom of the uplift tube, and terminates in a cyclone-like disengaging zone. From here the disengaged solids fall under gravity into a downcomer. An outlet tube is connected to a cyclone in order to prevent loss of particles to the environment.

Pressure sensors are placed at different heights on the tube, from which the local pressure drop of the suspension can be measured and thus the suspension void fraction calculated.

In operation, the DiFB is fluidised at a gas velocity U_f slightly higher than the minimum bubbling velocity. Pressurising the DiFB bed induces the solids to rise in the tube, transforming the system into an Upflow Bubbling Fluid Bed (UBFB). The operating parameters are the fluidisation flow rate of the dispenser fluidised bed (Q_f), the aeration flow rate in the tube (Q_{ae}) and the relative pressure of the DiFB freeboard (P_{fb}). Helium gas tracer was injected in the different gas injection points and the helium concentration was measured at the top of the bed as a function of time with a micro-volume thermal conductivity detector. Only 5% of the gas injected at the bottom of the fluidised bed travels up the transport tube since 95% is released through the pressure regulator valve. The helium tracing of the gas phase demonstrated that the gas flow in the transport tube is only upward.

The operating parameters of the reference test case are reported in Table 2.

Table 2: Operating parameters of the reference test cases.

Fluidisation flow rate (Q_f)	Aeration flow rate (Q_{ae})	P_{fb}
Q_f = 3.5-4.3 $Nm^3.h^{-1}$	150-225 $NL.h^{-1}$	15 kPa
U_f = 1.2-1.5 U_{mb}	U_{ae} = 2.5-7.5 U_{mb} (tube)	

Figure 3 shows the (single tube 30mm ID, circulating) experimental rig highlighting the measurement region.

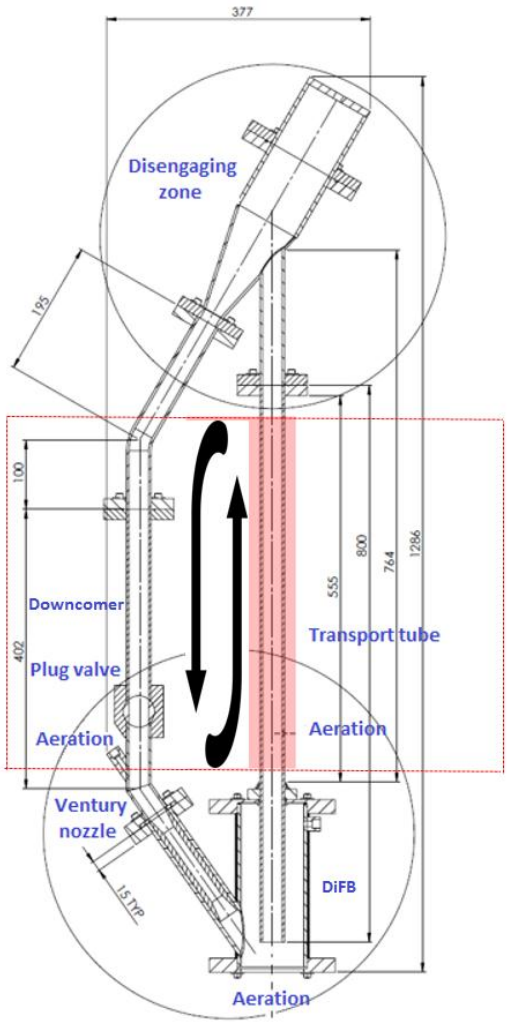

Fig 3. Detailed drawing of the experimental setup (Scale 1:4).

Figure 4 shows a photograph of the experimental apparatus and its arrangement during the PEPT experiments between the two detector arrays of the positron camera.

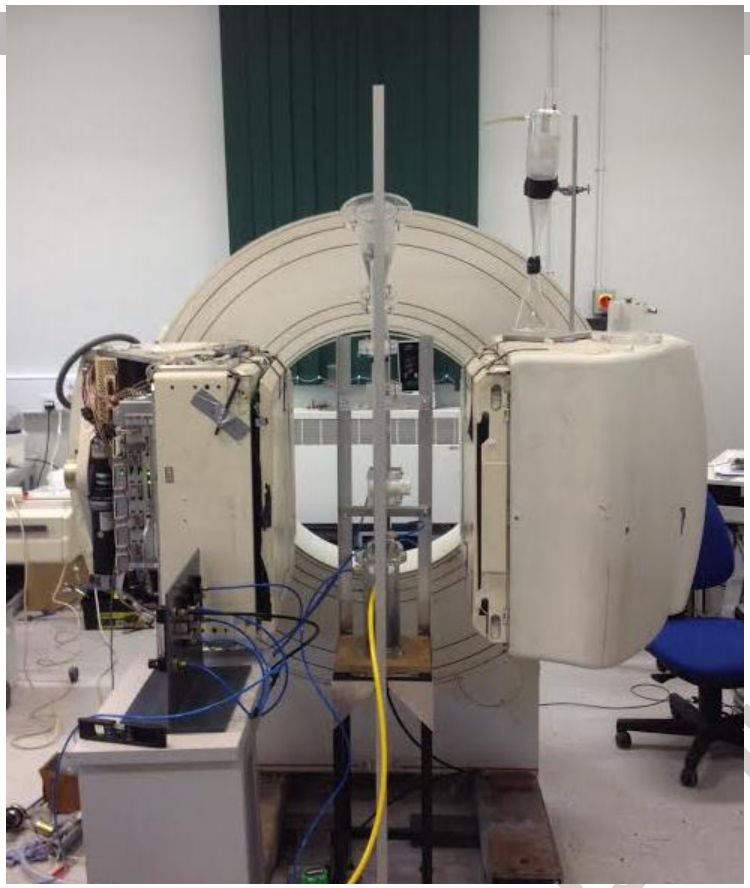

Fig 4. Location of the single tube circulating apparatus positioned relative to the PEPT camera.

Particles from the downcomer are fed into the pressurised DiFB continuously. Attempts were made to achieve this by use of a rotary valve. However, leakage problems were observed when connected in operation with the pressurised fluidised bed. A possible alternative was to use an L-valve but this was dismissed because a preliminary study showed that the pressure over the uplift transport tube made it very difficult to avoid gas leaking upwards through the L-Valve and associated moving bed downcomer. A purpose-designed inclined eductor (see Figure 5) in a 11 mm inner diameter recycling tube proved to be more satisfactory, limiting the flowpath of air up the transport tube but permitting the return flow of powder. This approach was adopted for all the experiments recorded here. The amount of air injected at the eductor throat was kept to the minimum necessary to move the bulk (48 NL/h). This was favoured by the static head of a dense column of particles maintained upstream which helped to overcome the ΔP requirement for flow. The conditions in the uplift transport tube, in particular density and particle velocity, were not determined by the conditions at the eductor but by the fluidising flow and by the additional aeration.

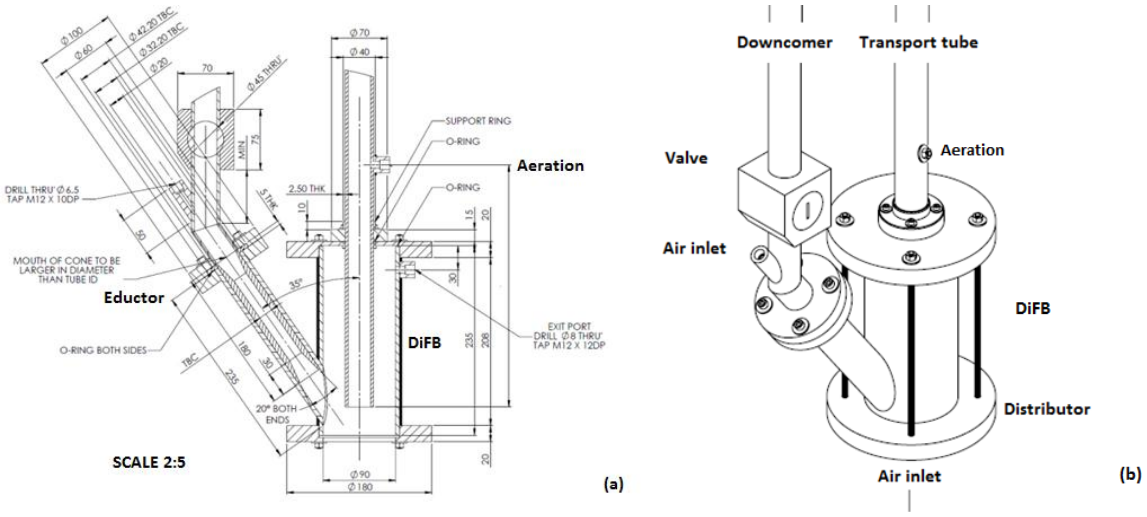

Fig 5. Schematics of the Eductor and DiFB (a) Engineering drawing Scale 2:5; (b) 3D view of the system.

The advantages of the eductor are multiple because its throat acts as a restriction on the gas flow, reducing the velocity at the downstream solids entry end; these advantages include a favourable pressure range, dense phase operation, no blowback, no mechanical shearing and absence of moving parts. The system included a mechanical seal (a PTFE plug valve) upstream of the eductor to shut off backflow during the start-up and permit a dense static bed to accumulate in the return tube. The rig was also equipped with a pressure control system and a data logger connected to a LabVIEW interface (National Instruments Corporation) in order to obtain pressure readings using pressure transducers at different points in the uplift transport tube. If the system is not fully controlled it can lead to erratic pressure fluctuations in the fluid bed and air can travel up the recycle tube in a slug flow pattern, fluidising powder back up the recycle tube to the disengagement section; bridging of powder can also occur in the recycle tube due to this effect.

A regulated air supply from a compressor provided a constant pressure supply (300 kPa). The air was introduced to the system through a sintered brass distributor plate with a pore size of 37 µm and a thickness of 6 mm (GKN Sinter Metal Filters GmbH) in order to achieve a homogeneous flow of gas through the full cross section of the DiFB.

For purposes of experimental repeatability and to reach steady-state conditions, it was important to satisfy the condition that the overall mass circulation was in the desired range. This was achieved by using variable area flowmeters connected to the flow loop using large bore flexible piping (8 mm OD) and avoiding over-pressurising the system (controlling the pressure drop along the uplift transport tube and using a back pressure regulator set to control pressure in the emitting fluidised bed at approximately 110 mbar). Analysis revealed a direct correlation between the extent of aeration and the solids mass flow rate. During these experiments the average solids flow rate was 70 kg/h with a particle volume fraction of 25-40%.

3. Results and discussion

3.1 Influence of the operating conditions

To establish the operating conditions for stable upward suspension flows the governing parameters including aeration flow rate of the uplift transport tube, air flow in the venturi and fluidisation flow rate were appropriate to ensure steady flow of solid in the tubes and comparable with results obtained in the previous work (Boissiere et al., 2015). The flow in the vertical tubes is greatly influenced by the fluidisation flow rate of the DiFB. The fluidisation velocity must be higher than the minimum bubbling velocity to warrant an acceptable stability. The optimal fluidisation velocity ranged between 1 and 1.4 Umb to ensure a steady flow of solid in the tubes. Therefore, the reference value was chosen as 1.2 Umb (0.096 m/s). Moreover, it was demonstrated that the same aeration and fluidisation conditions ($U_f > U_{mb}$ and $U_{ae} > 5\ U_{mb}$) are required to ensure stability. A successful reproducible operating regime was achieved, together with a high particle volume fraction which is important for good heat transfer.

The influence of the aeration flow rate on the local void fraction above the aeration tap was evaluated, using the pressure drop over a section of the pipe to deduce the void fraction. Pressure sensors were placed along the transport tube (y=100 and 300 mm). Figure 6 gives the local void fraction calculated from Equation 1. This equation expression is obtained by making a balance between the drag force and buoyancy by neglecting the fiction of the particle at the wall (Boissiere, 2015).

$$\varepsilon = 1 - \frac{\Delta P_{hydro}}{(\rho_p - \rho_g) \cdot g \cdot L_c} \qquad (1)$$

As expected, the void fraction in the tube increases with the aeration flow rate. Due to the short distance between the aeration tap and the disengaging zone in this apparatus the void fraction is barely affected by the height, and low effect of gas expansion is observed in this case due to the pressure loss.

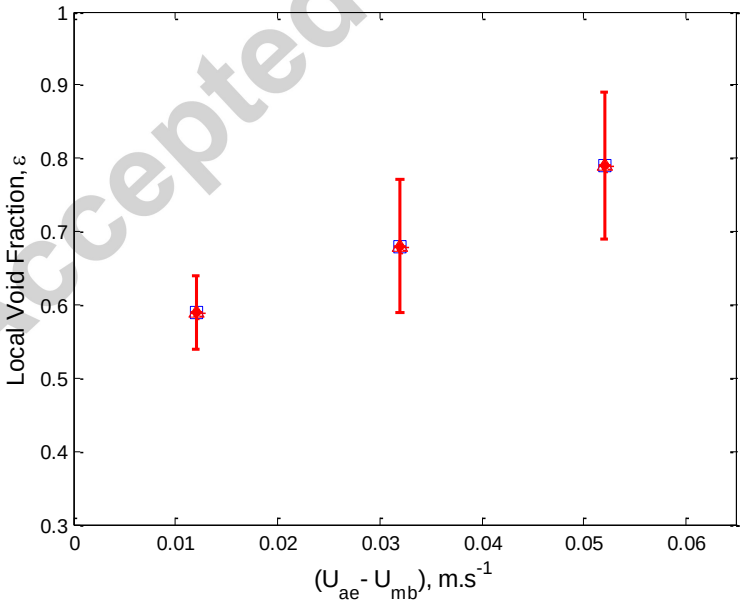

Fig 6. Effect of aeration flow velocity on the local void fraction.

3.2 Study of the particle trajectories using PEPT

Positron Emission Particle Tracking (PEPT) is a non-invasive technique which uses a single radioactive particle as a tracer within the fluidised bed (solar receiver tube). The tracer is either identical to or similar in properties to the particles found within the bed in order to avoid any difference in fluidisation properties (similar approaches in other applications are given by Parker et al., 1993; Garcia-Triñanes et al., 2014; Valdesueiro et al., 2015). The tracer particle was treated with the isotope fluorine 18 (^{18}F), which emits positrons without any emission of gamma radiation. The single tracer was then mixed with other SiC particles and added to the DiFB. A Geiger counter was used to detect the particle as it entered the uplift transport tube and to check that the tracer particle was circulating. The tracer was then located by triangulation of gamma rays arising from the annihilation of the emitted positrons, each location being calculated from ~100 such gamma-ray pairs.

The PEPT tracking experiments were mostly carried out over a 1 m length of the tube starting from the top of the DiFB; the distance from the lowest detection point to the distributor in the experiments reported here is 300 mm (so that the DiFB is below the field of view). The conditions reported here matched the highest solids flowrate reported in related work on a large scale pilot rig (Flamant et al., 2013), corresponding to a specific flow rate of 25 kg/m^{2}s and an aeration flowrate of 250 NL/h (U_{ae}-U_{mb}=0.052 m/s).

The raw PEPT data are in the form of a list of x, y, z, time tracer particle coordinates. Each location is accompanied by an attributed error, which is calculated from the set of gamma-rays giving rise to that location. Before the PEPT data can be used for further analysis, outlying gamma-ray pairs are eliminated in order to remove spurious data. An algorithm is available for doing this systematically but some user intervention is possible in order to refine the selection, taking account of the experimental geometry, tracer activity level and experimental conditions such as typical tracer velocity. f is defined as the fraction of events remaining after removing the gamma-ray pairs which are furthest from the point which has the minimum perpendicular distance from all the trajectories. Using a higher value of f will increase the number of locations made per unit time, but if the f used is above the optimum these values will have a higher error.
For a set of N detected events, with a fraction f used to locate the tracer, the precision Δ of locating a stationary particle is given by:

$$\Delta \approx \frac{w}{\sqrt{fN}} \qquad (2)$$

where w is the spatial resolution of the camera (Seville et al., 2009) . It can be seen that the value of Δ can be made arbitrarily small by making N sufficiently large. Over a long enough time scale (increasing N) a stationary particle can then be located arbitrarily well.
The processed data of a stationary particle has also been explained to show correlation with processed data from a moving particle therefore a stationary file was recorded and processed. Figure 7 shows that the combined standard deviation of x,y,z coordinates (3D) for this particular set up is almost constant at f values of 0.3-0.5 (30-50%) and N=250. For this particular set of data the standard deviation of the error is measured as 0.59 mm and the mean error is 0.85 mm (3D). E represents the standard deviation of the error. This value remains fairly constant with an ‘f’ value greater than 20.

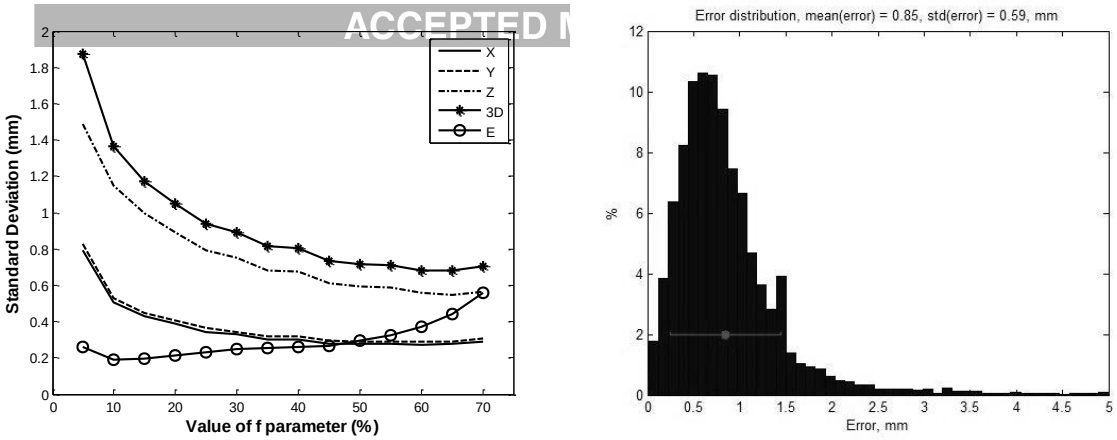

Fig 7. Combined standard deviation of x,y,z coordinates (3D) as a function of the f parameter.

Once the parameters of the algorithm are selected, the tracking of a tracer particle for an extended period of time in a closed, circulating system builds up an integrated picture of particle behaviour at each point in space and this allows the visualisation of the particle behaviour and reconstruction of maps of axial and radial movement, circulation times and pseudo-density (using the PEPT occupancy function). The mean interval between successive locations is approx. 20 ms with a very small increase over the duration of the experiment due to the decay of the tracer particle activity. In general the quality of data is extremely high and PEPT is working well within its capabilities as regards measurement of particle location, and hence velocity. Particle velocities are calculated considering the "six point" method producing an estimate of the tracer velocity at every point of its path which reduces the error on the results (Stewart et al, 2001).

3.3 Flow structure and solids motion

The overall behaviour of the bulk material can be deduced from analysis of the tracer particle motion. This is applicable provided that the experiment covers a long enough time scale such that the tracer particle exhibits the full range of motion and visits all possible locations in the experimental apparatus a sufficient number of times.

Examples of the excellent location accuracy are given in the following graphs. Figure 8 depicts the vertical coordinate in several different passes. The blanks between successive vertical passes correspond to the time interval spent by the tracer in the rest of the uplift transport tube and in the external recycle loop. Figure 9 shows the increase in the number of cycles per hour as a function of the aeration rate, other conditions held constant. At each condition, the cycle frequency varies by less than ±3%. Note that at U_{ae}=0, no circulation occurs. The cycle time is dominated by the period outside the transport tube, so that the effect of increased aeration is limited.

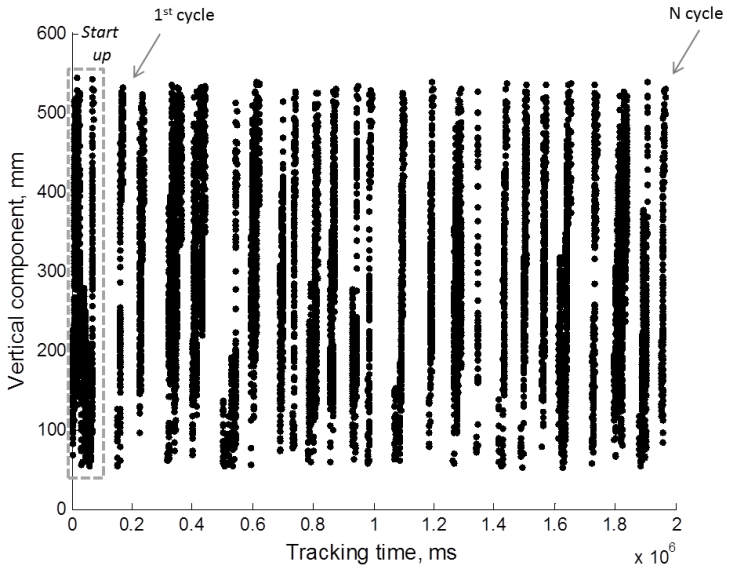

Fig 8. Vertical coordinate against time during several passes.

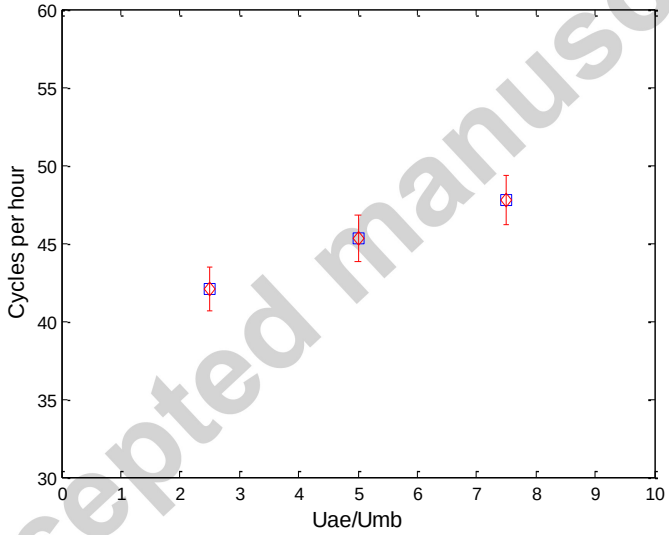

Fig 9. Average number of cycles per hour using (Uae =0.02,0.04,0.06 m/s)

Figure 10 shows a typical example of a tracer particle vertical trajectory where y is the vertical coordinate with respect to the centre of the PEPT camera and x,z are the horizontal coordinates. Vertical jumps are probably associated with particles that are carried by bubbles, as investigated in previous work on bubbling fluidised beds (Stein et al., 2000; Wong, 2006; Lam Cheun U, 2010).

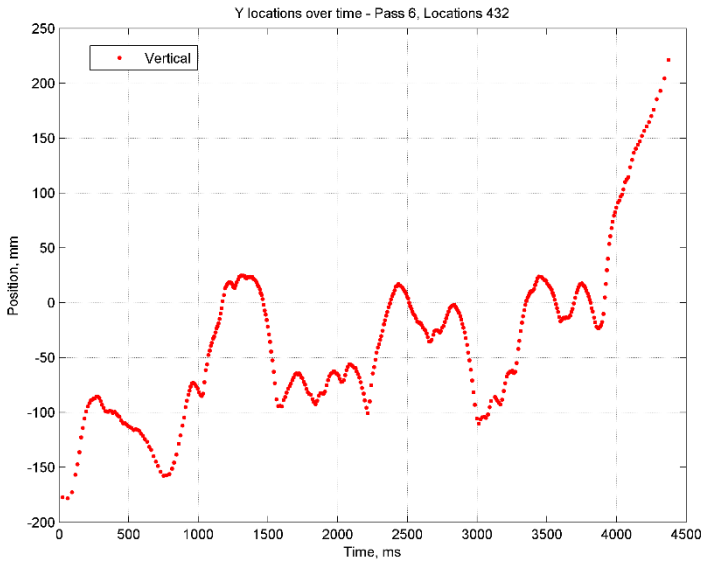

Fig 10. Example of individual trajectory against time (Uae=0.04 m/s).

Stein et al. (2000) showed that in bubbling beds, rapid and prolonged vertical movements are directly correlated with bubble rise velocity. Particles are picked up in the wakes of bubbles and rise a certain distance at the bubble velocity before falling out of the wake. They then experience a quiescent period (the “idle time”) before being picked up by another bubble, which may move them further up the tube.

In order to estimate the bubble velocities from the PEPT trajectories, “jump” velocities were obtained by selection of portions of trajectory satisfying criteria of sustained vertical movement, as described by Stein (2000). Fig 11 shows the results, averaged over the column cross-section, as a function of vertical distance above the tube entrance. Note that the aeration point is at 250 mm above the bottom of the tube. Two different minimum distance criteria were used: the vertical distance travelled by the particle must be at least 50 mm or 100 mm and the tracer particle must be moving upwards continuously over that distance. The results show that the values obtained from PEPT data are in close agreement with predicted bubble rise velocities.

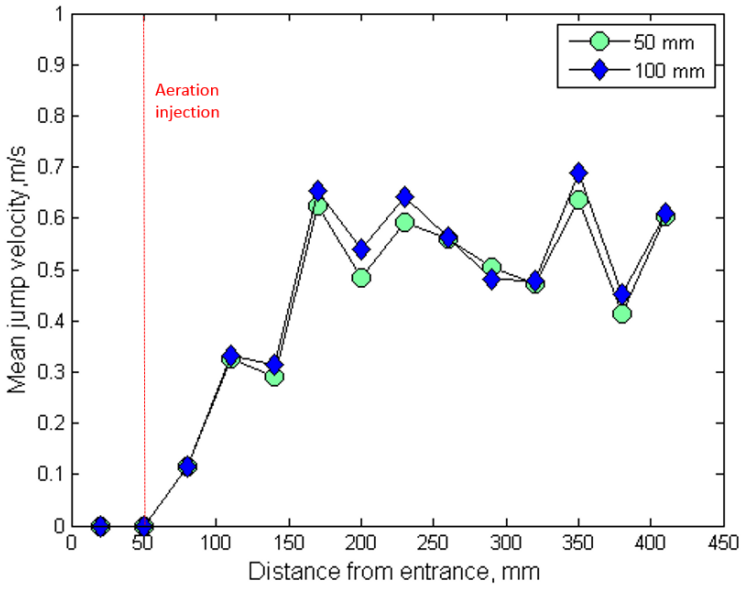

Fig 11. Mean jump velocity of the tracer particle (Uae=0.04 m/s).

Figure 12 shows a set of twenty "jump" trajectories within the tube, showing the start of jump and the variation in behaviour and average velocity. The tracer comes down continuously close to the wall following a different mechanism.

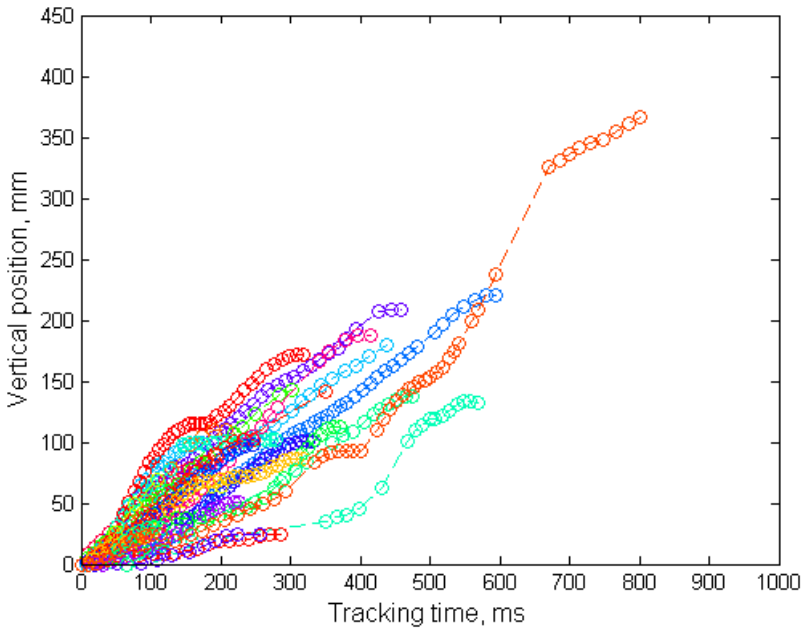

Fig 12. Examples of rapid upward vertical motion of the tracer particle (Uae=0.04 m/s).

The general pattern of the bulk movement of solids is upward movement in the centre of the bed and downward movement at the walls, which is typical for fluidised beds as the bubble motion concentrates towards the centre (Seville, Tuzun & Clift, 1987). Figure 13 illustrates this effect by plotting the relative number of trajectories moving upwards and downwards as a function of radius, normalising for the areas of the annuli considered.

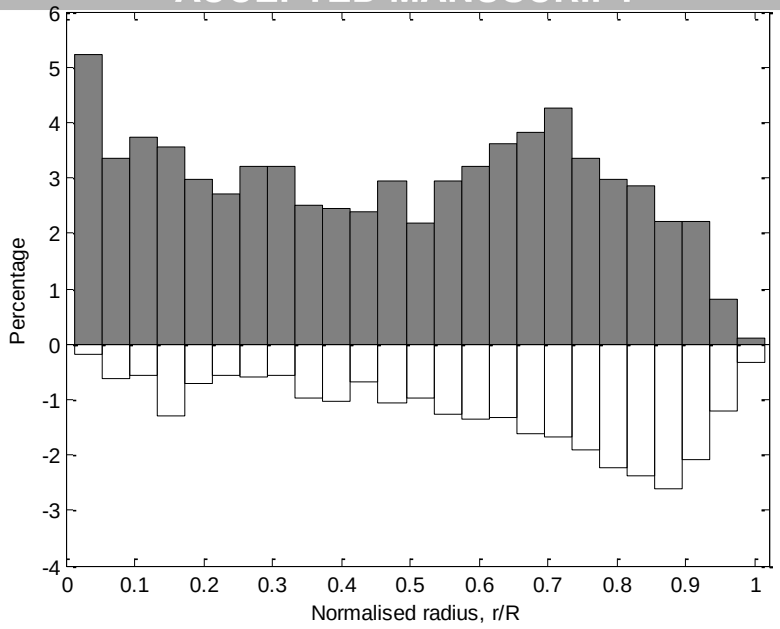

Fig 13. Number of trajectories over radius normalised by area for the region 200 mm above aeration- Uae=0.04 m/s (Grey, rising trajectories- White, Falling trajectories).

Figure 14 shows the same data plotted to show the locations of upward and downward trajectories in plan view.

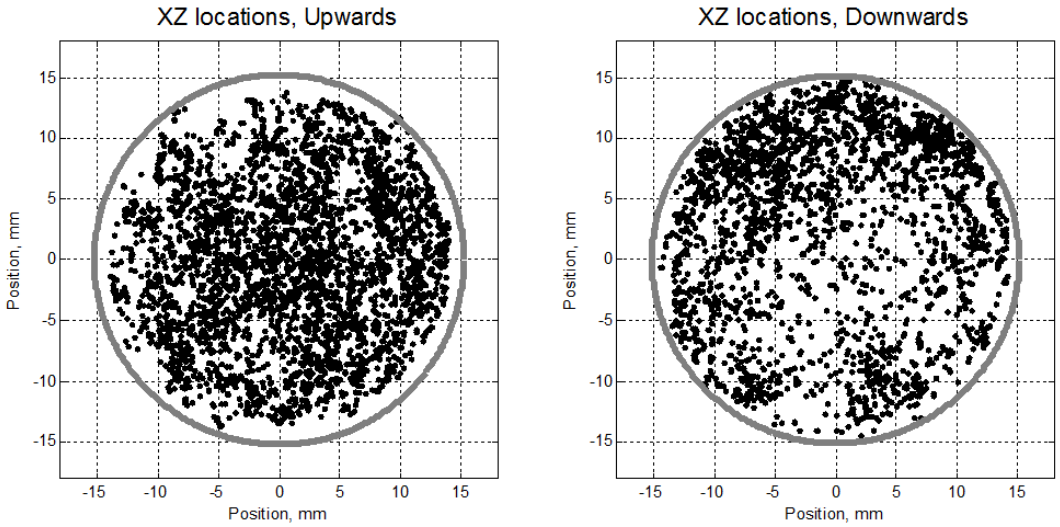

Fig 14. Locations according to the direction of particle movement considering a section between y=100 mm and 300 mm (Uae=0.04 m/s).

Figures 13 and 14 are evidence of internal circulation in the tube, which favours heat transfer, enabling individual particles to interact with the wall and then move to the centre of the tube and exchange heat with fresh particles that are moving upwards.

3.4. Axial velocity profiles

Velocity calculations for PEPT data were performed using the standardised six-point method, introducing some smoothing (particularly in chaotic/turbulent systems) but reducing the overall error.

Figure 15 shows the distribution of the vertical component of the velocity (V_y) for trajectories passing through a region of interest in the central part of the uplift transport tube above aeration (arbitrary height of 200 mm from the aeration point) using a normalised radius.

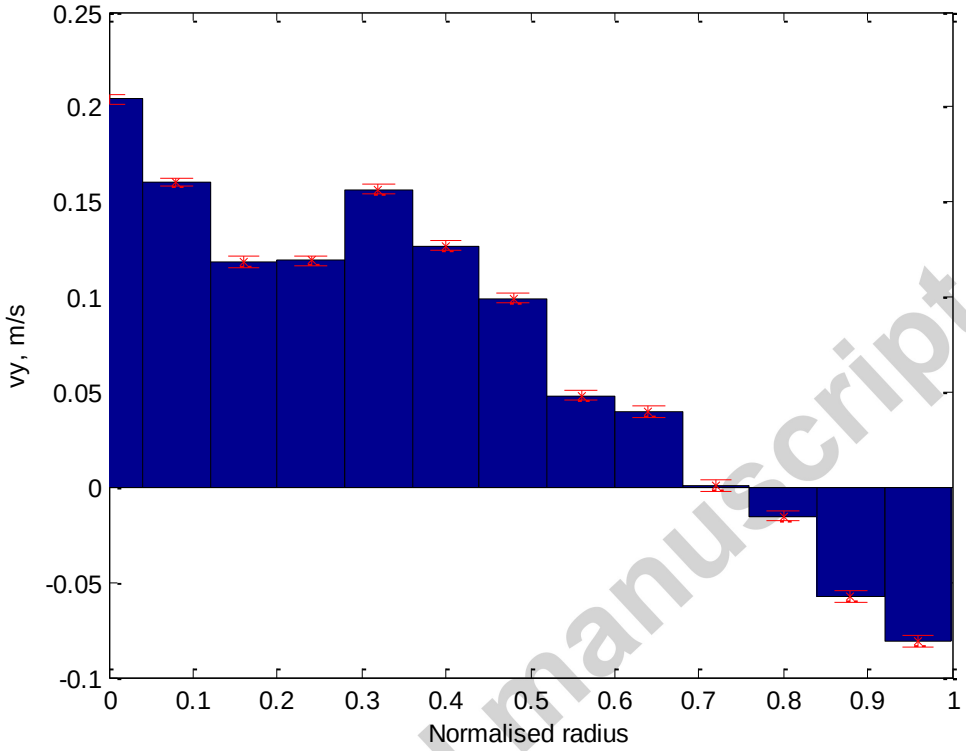

Fig 15. Average and distribution of vertical velocity with radial position considering a section between y=100 mm and 300 mm (Uae=0.04 m/s).

Vertical components of the velocity vectors are averaged per bin. The error bars represent the standard deviation divided by the square root of the number of observations of the sample. Note that both positive and negative velocities are present at all radii. The mean values again demonstrate upwards motion in the centre of the uplift transport tube and downward motion near the walls.

3.5 Solids mixing and dispersion

Particle trajectories provided by the analysis of PEPT data can also be used to characterise solids mixing and calculate dispersion rates. The continuous trajectory can be cut up into many shorter trajectories, each having its origin in the same reference position (Martin et al., 2007). This is equivalent to tracing the path of many particles from the same location simultaneously (known as the principle of ergodicity). In order to achieve this, each point on a trajectory can be taken as a starting point and the tracer's subsequent displacement observed over time.

Figure 16 shows the average timing between six successive locations, showing the expected near linearity.

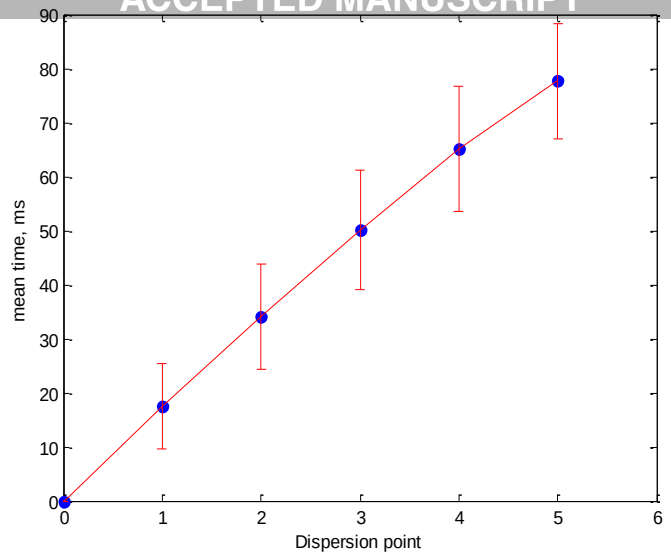

Fig 16.Mean time interval between six successive locations.

If several trajectories start at the same point, the distribution of their end points at some specified later time can be obtained. The width of the distribution of their displacements from the starting point is conveniently expressed as mean of mean displacement squared $(disp\text{-}disp_{mean})^2$.

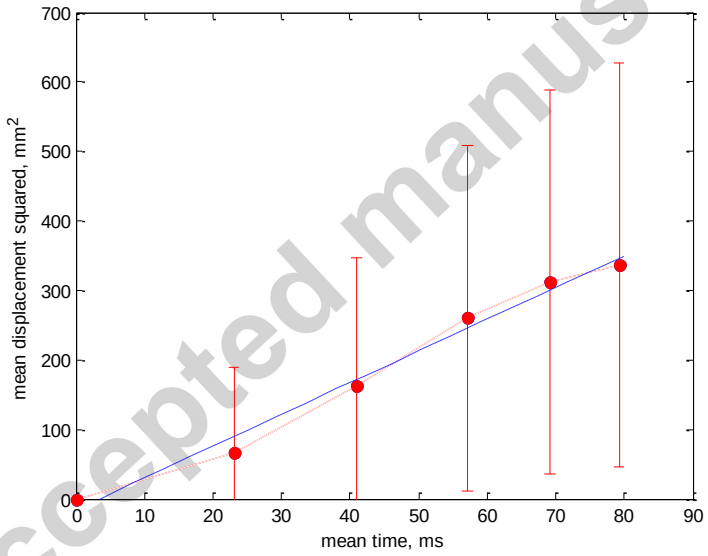

Fig 17. Mean displacement squared against time for all the tracks of a set of experiments.

A diffusive model of axial dispersion would predict that the mean value of $(displacement)^2$ increases linearly with time and is proportional to the axial dispersion coefficient, D given by:

$$x_d^2(t) = 2Dt \qquad (3)$$

where $x_d(t)$ is the axial distance moved by the tracer from the starting location after time t and $x^2_d(t)$ represents the mean squared axial displacement of the tracer after time t.

Figure 18 shows the change in variance of vertical displacement of the tracer particle with time after it crosses the reference line (used as the starting location of the particle). The linear, middle part of the graph which shows the max gradient usually with an R value of at least 0.99 is used to calculate the dispersion coefficient.

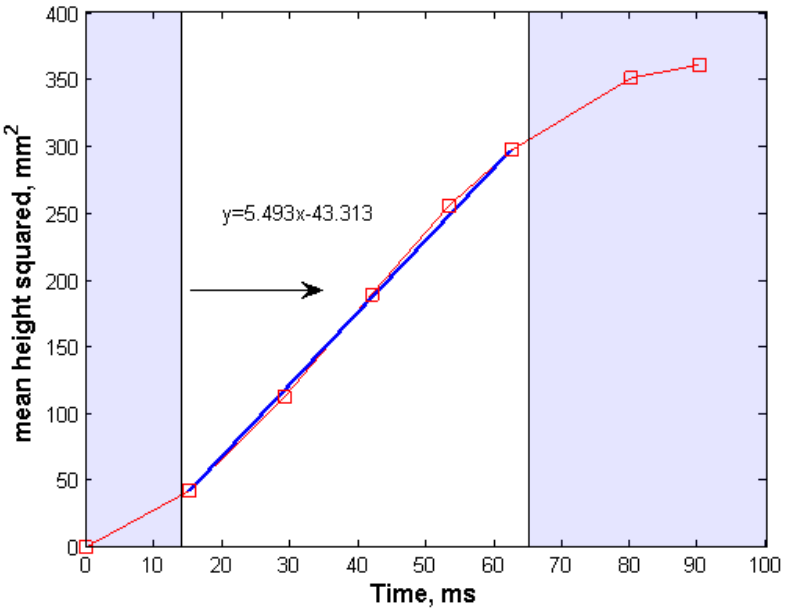

Fig 18. Mean displacement squared against time after the particle crosses the reference plane which is 200 mm above the aeration inlet (Uae=0.04 m/s).

The data indeed shows behaviour which closely approximates to the expected linear relationship. The corresponding dispersion coefficients are shown for various operating conditions in Figure 19.

The dispersion coefficient was calculated from a continuous trajectory of one particle, considering different reference planes above the aeration level. The path of the tracer particle was tracked from the time at which it crossed the fixed reference.

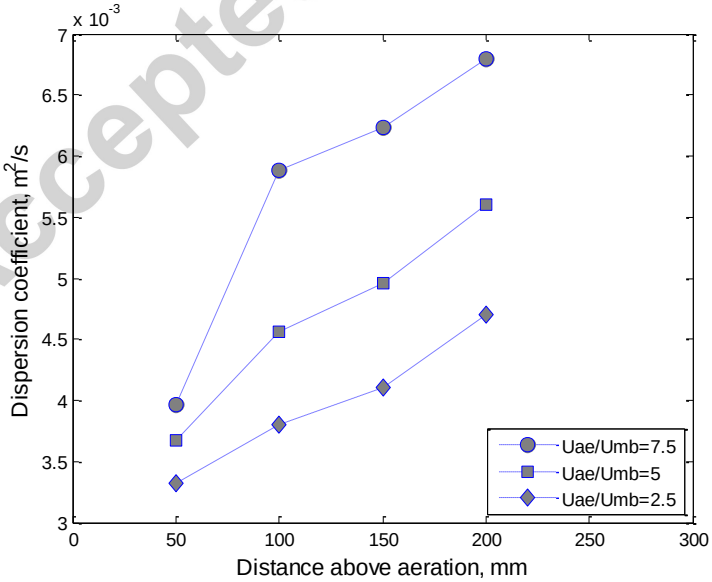

Fig. 19 Variation of the axial dispersion coefficient with height at different aeration velocities.

As expected, the dispersion of the tracer increases with vertical position above the aeration point. The magnitude of the axial dispersion coefficient appears to be higher in this system than the values

reported in the literature using PEPT as particle tracking method for bubbling fluidised beds. In an early study using ferromagnetic particles, Avidan and Yerushalmi (1985) reported that the axial dispersion coefficient calculated using the contercurrent flow model increased with gas velocity. Moustafi and Chaouki (2001) showed that the superficial gas velocity and the axial velocity gradient have a significant effect on the solid diffusivity. Lam Cheun U using PEPT reported a maximum value of 0.005 m^2/s at different superficial gas velocities. The calculation of the axial solids dispersion coefficient has also been addressed by Zhang (2009) using a steady-state gas tracer. It is worth noting that these values are considerably affected by the superficial gas velocity.

Table 3: Dispersion coefficients in various systems by different authors.

Particle	Average Particle size	System	Authors	D (m^2/s)
FCC	49 µm	BFB/Ferromagnetic tracer	Avidan and Yerushalmi (1985)	0.075-0.15
FCC	70 µm	BFB[1]/RTP[2]	Moustafi and Chaouki (2001)	0.001-0.06
FCC	78 µm	FFB[3]/Gas tracer	Zhang et al (2009)	0.01-0.12
Al_2O_3	48 µm	BFB/PEPT	Lam Cheun U (2010)	0.001-0.005
SiC	64 µm	UBFB[4]/PEPT	This work	0.003-0.007

3.6 Vertical solid mass flux in the tube

The axial flux (vertical component) kg/m^2s was calculated using a new approach that takes into account the number of times that the tracer crosses an arbitrary boundary in the desired direction (n_{up} or n_{dwn}), the mass of the particles, the area of the boundary considered and the sampling time. Radial profiles of vertical solid mass flux (kg/m^2s) were obtained using Equations (4) and (5) at a reference height of 200 mm taking into account the total mass of particles circulating (M_{part}), the sampling time ($t_{sampling}$) and A_n representing the cross sectional area of the radial element considered (m^2):

$$G_{up} = \frac{M_{part}.n_{up}}{A_n \cdot t_{sampling}} \quad (4)$$

$$G_{dwn} = \frac{M_{part}.n_{dwn}}{A_n \cdot t_{sampling}} \quad (5)$$

Figure 20 presents radial profiles above the aeration level of solids mass flux (upward and downward) for the reference aeration velocity (0.04 m/s), again showing higher upward mass flux in the core region of the uplift transport tube.

[1] BFB Bubbling fluidised bed
[2] RTP Radioactive particle tracking
[3] FFB Baffle-free fluidised bed
[4] Upflow Bubbling Fluid Bed

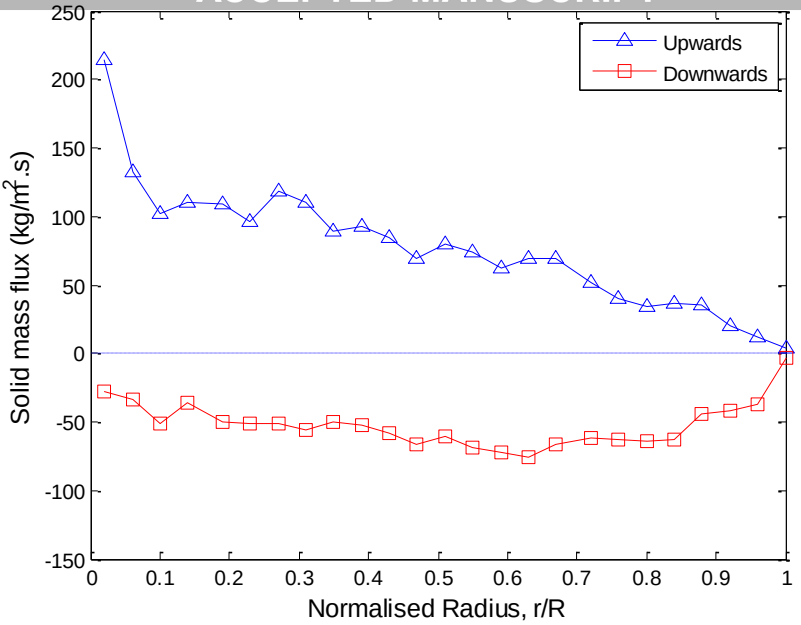

Fig 20. Radial profile of the upward and downward solids mass flux at a reference height of 200 mm (Uae=0.04 m/s).

In order to calculate the net solid flux considering annuli of equal area, the number of times that the tracer appears in the zone (height of interest and radius of interest) for each track is computed considering the vertical crossing of boundaries and the direction vector for upwards and downwards trajectories through the volume elements taking into account the total sampling time.

The result of integrating over the whole cross-section gives the net up and down flux and it can be found in Figure 21.

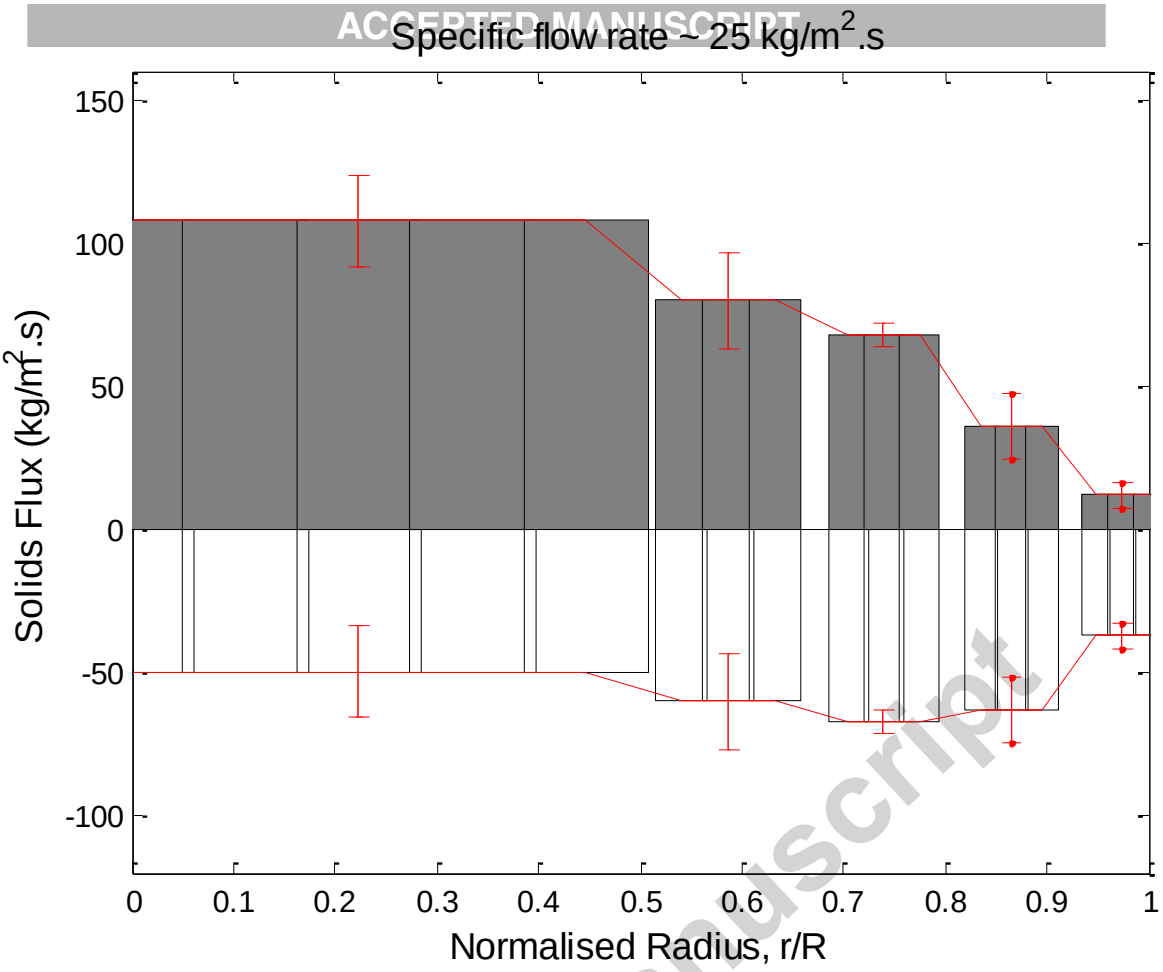

Fig 21. Solids flux considering cylinders of equal area considering a section between y=100 mm and 300 mm (Uae=0.04 m/s).

Inspection of this graph confirms that there is net upflux over the whole cross-section and downflux near the wall.

4. Conclusions

A new pilot plant has been set up in continuous operation to provide a complete understanding of the hydrodynamics and particle motion in upward flowing dense particle suspensions. This small scale circulating apparatus with upward dense flow uses an eductor and simulates the flow in a single solar collector tube.

Positron emission particle tracking (PEPT) has been demonstrated to be a technique that can reveal detailed and relevant information about the particle circulation within the uplift transport tube. Under the operating conditions reported here the flow in the transport tube is upwards in the centre and downwards at the wall. This was particularly noticeable in a region situated 200 mm above aeration when using Uae=0.04 m/s since the upwards trajectories represented 70 % of the total.

Analysis of the PEPT data provides valuable information on the particle trajectories, axial velocity profiles, void fraction (25-40 %), vertical solid mass flux (25 kg/m^{2}s) and dispersion coefficients. The calculated axial dispersion coefficients are in the range reported by other earlier studies working with higher velocity systems.

Future experiments will investigate how the results of this study help to provide experimental evidence of how the radial movement of particles controls the suspension effective thermal conductivity, thus the heat transfer from the wall to the dense suspension of particles.

Nomenclature

PEPT	Positron Emission Particle Tracking
^{18}F	Fluorine-18 radioisotope fluorine
UBFB	Upflow Bubbling Fluid Bed
DiFB	Dispenser Fluidised Bed
λ	Thermal conductivity, W/mK
C_p	Specific heat capacity of the solid, kJ/kgK
T_{melt}	Melting point of solid K
T_{max}	Solid sintering temperature K
ΔP_{bed}	Bed hydrostatic pressure
U_g	Superficial gas velocity, mm/s
U_{mf}	Minimum fluidisation velocity, mm/s
U_{mb}	Minimum bubbling velocity, mm/s
U_{ae}	Aeration superficial gas velocity, mm/s
u_{ae}/U_{mb}	Aeration velocity/bubbling velocity mm/s
ε	Void Local void fraction
ΔP_{hydro}	Hydrostatic gas pressure drop, mbar
L_c	Tube measurement length
A_c	Cross sectional area of the tube, m^2
ε_{mf}	Void fraction at minimum fluidisation
ε_{mb}	Void fraction at minimum bubbling
ρ_p	Solid particle density, kg/m^3
d_p	Average Solid particle diameter, µm
Q_f	Fluidisation flow rate, Nm^3/h
F_p	Solids feeding flow rate, kg/h
Q_{ae}	Aeration flow rate, Nm^3/h
Q_{bt}	Air flowrate exchanged between the dispenser bed and the tubes, Nm^3/h
D	Axial dispersion coefficient m^2/s
P_{fb}	Pressure of the dispenser bed freeboard, mbar
N	Number of events
w	Spatial resolution of the camera
Δ	Precision of locating a stationary particle
f	Fraction of events used to locate the tracer
G_{up}	Upwards solid flux, kg/m^2s
G_{dwn}	Downwards solid flux, kg/m^2s
n_{up}	Number of events crossing the section (with positive velocity)
n_{dwn}	Number of events crossing the section (with negative velocity)
M_{part}	Total mass of particles circulating, kg

Acknowledgements

This work was developed in the frame of the CSP2 Project - Concentrated Solar Power in Particles. This project has received funding from the European Union's Seventh Programme for research, technological development and demonstration under grant agreement N° 282 932. The authors would like to thank Strata Technology Ltd for their assistance in the design and manufacturing of the GU1 mock up.

References

Flamant, G., Hemati, M. French Patent No. 1058565, 20 October 2010. PCT extension, 26 April 2012, No. WO 2012/052661 A2.

H. T. Bi, J. R. Grace (1995). "Flow regime diagrams for gas-solid fluidization and upward transport." International Journal of Multiphase Flow, 21, 6, 1229-1236

Flamant, G., Fatah, N., Filtris, Y. (1992) "Wall-to-bed heat transfer in gas-solid fluidized beds: Prediction of heat transfer regimes ".Powder Technology, 69 (3), 223-230

J. S. M. Botterill, (1975) 'Fluid-bed heat transfer. Gas fluidized bed behaviour and its influence on bed thermal properties', Academic Press, New York.

B. Boissiere, R. Ansart, D. Gauthier, G. Flamant, M. Hemati, (2015) "Experimental hydrodynamic study of gas-particle dense suspension upward flow for application as new heat transfer and storage fluid". Canadian Journal of Chemical Engineering, 93 (2), 317-330

G. Flamant, D. Gauthier, H. Benoit, J.-L. Sans, B. Boissière, R. Ansart, M. Hemati, (2014) "A New Heat Transfer Fluid for Concentrating Solar Systems: Particle Flow in Tubes". Energy Procedia, 49, 617-626

D.J. Parker, C.J. Broadbent, P. Fowles, M.R. Hawkesworth, P.A. McNeil (1993) 'Positron emission particle tracking—a technique for studying flow within engineering equipment', Nucl. Instrum. Methods in Physics Research Section A, Vol. 326 (3), 592-607

J.P.K. Seville, A. Ingram, X. Fan, D.J. Parker, (2009) 'Positron Emission Imaging in Chemical Engineering', Jinghai Li, Editor(s), Advances in Chemical Engineering, Academic Press, Chapter 4 Vol. 37, 149-178

Garcia-Triñanes P., Valdesueiro D., Seville J.P.K., Meesters G.M.H., Kreutzer M.T., van Ommen J.R. Gargiuli J. 'Enhancing the activation of silicon carbide particles with gas-phase coating of aluminium oxide'. 7th World Congress on Particle Technology (2014), Beijing, China

D. Valdesueiro, P. Garcia-Trinanes, G.M.H. Meesters, M.T. Kreutzer, J. Gargiuli, T. Leadbeater, D.J. Parker, J. Seville, J.R. van Ommen "Enhancing the activation of silicon carbide tracer particles for PEPT applications using gas-phase deposition of alumina at room temperature and atmospheric pressure". Nuclear Instruments and Methods in Physics Research Section A. To be published-2015

G. Flamant, D. Gauthier, H. Benoit, J.L. Sans, R. Garcia, B. Boissière, R. Ansart, M. Hemati (2013) "Dense suspension of solid particles as a new heat transfer fluid for concentrated solar thermal plants: On-sun proof of concept", Chemical Engineering Science, 102, 567-576

Seville, J.P.K., Ingram, A., Fan, X., Parker, D.J., (2009) "Positron emission imaging in chemical engineering", Advances in Chemical Engineering 37 (Li, J, ed.) Elsevier, Amsterdam. ISSN: 0065-2377

R.L. Stewart, J. Bridgwater, Y.C. Zhou, A.B. Yu, (2001) "Simulated and measured flow of granules in a bladed mixer—a detailed comparison", Chemical Engineering Science, Vol. 56, (19), 5457-5471

M. Stein, Y.L. Ding, J.P.K. Seville, D.J. Parker (2000) "Solids motion in bubbling gas fluidised beds", Chemical Engineering Science, Vol. 55 (22), 5291-5300

Y.S. Wong, (2006), "Particle motion in relatively thin fluidised bed models". Chemical Engineering Science, Vol. 61 (18), 6234-6238

Lam Cheun U, You Van (2010) "Solids motion in fluidised beds of fine particles". Ph.D. thesis, University of Birmingham

J. Seville, U. Tüzün, R. Clift (1987) "Processing of particulate solids". Series: Particle Technology Series, Vol. 9 (Springer)

T.W. Martin, J.P.K. Seville, D.J. Parker, (2007) 'A general method for quantifying dispersion in multiscale systems using trajectory analysis', Chemical Engineering Science, Vol. 62 (13), 3419-3428

A. Avidan and J. Yerushalmi, (1985) "Solids mixing in an expanded top fluid bed", AlChE Journal, Vol. 31, No. 5, 835-841

Mostoufi, N., Chaouki, J, (2001) "Local solid mixing in gas–solid fluidized beds", Powder Technology, Vol. 114, 23–31

Zhang, Y., Lu, C., Shi, M., (2009) "Evaluating solids dispersion in fluidized beds of fine particles be gas backmixing experiments". Chemical Engineering Research and Design, Vol. 87, 1400-1408.

Figure Legends

Fig 1. Scanning electron microscopy picture corresponding to the SiC powder sample.

Fig 2. Particle size distribution of the SiC powder.

Table Legends

Highlights

- **An experimental apparatus for the investigation of hydrodynamics of upward-flowing dense phase particle suspensions.**
- **The effect of fluidisation and aeration flow rate on solid flow stability is presented.**
- **PEPT was used to visualize particle trajectories and velocity profiles.**
- **A novel procedure was used to obtain vertical solid flux.**